The VIMS Wavelength and Radiometric Calibration

Roger N. Clark[1], Robert H. Brown[2], Dyer M. Lytle[2]

[1] Planetary Science Institute, Lakewood, CO, 80227
[2] Department of Planetary Sciences, University of Arizona, Tucson, AZ, 85721

NASA Planetary Data System
Version 1.20
10/05/2016

Abstract

We derive a new radiometric calibration for the Visual and Infrared Mapping Spectrometer (VIMS) on Cassini. Since entering orbit in 2004, the VIMS instrument has undergone small shifts in the wavelength calibration of the spectrometer. The maximum shift is currently 10.4 nm (0.65 channels) and is estimated to be 0.71 channels at the end of mission. The wavelength shifts now require a time-dependent radiometric calibration technique to be deployed to preserve radiometric accuracy. Herein we quantify the time-dependent wavelength shift, and describe a compensatory scheme that will provide an accurate calibration for both specific intensity and I/F for VIMS measurements made during the Cassini Mission.

Introduction

The radiometric responsivity of a spectrometer or imaging instrument is complex, depending upon many factors, some of the most important being the aperture collection area, spectral transmission of the optical system, and the response function of the detector(s). The VIMS is an imaging spectrometer (Miller *et al.*, 1996, Brown *et al*., 2004) whose spectral responsivity varies with angular position in the field of view and with wavelength. The IR chanel primary optical design incorporates Ritchey Cretien foreoptics, a reverse-Dahl-Kirkham collimator with a large central obscuration, a triply blazed reflection grating, Cassegrain camera optics and a linear, 256-element array of InSb detectors overlain with 4 order-sorting/thermal-blocking filter segments. The VIS channel uses an off-axis Shafer telescope with an Offner design spectrometer. The flat-field response of the instrument varies with wavelength, and a flat-field image cube with 352 wavelengths is thus employed to correct the system response over the field of view relative to the instrument's boresight pixel. The spectral bandpass of the instrument also varies slightly across the full range of VIMS' spectral response, adding to the complexity of the calibration. Additional issues arise due to ringing in the instrument response function driven primarily by the blocking/order-sorting filters on the VIMS focal plane (in some cases ±10% or more [Figure 1]). Because of the ongoing wavelength shifts in the instrument, relative to when the instrument response function was measured on the ground and after the Cassini Jupiter flyby in late 2000, artifacts in radiometrically calibrated spectra result because the response function at any later time is actually sampled at different wavelengths than the wavelength set used in the ground measurements. The resulting artifacts are primarily caused by the use of a response function in multiplicative or divisive operations sampled using the original, ground wavelength set, and then used to calibrate to specific intensity or I/F instrument data obtained at a later time and consequently done with a different set of wavelengths. Below we describe our methodology to track the shifting wavelengths, and then apply a time-dependent, radiometric calibration that compensates for all the known effects.

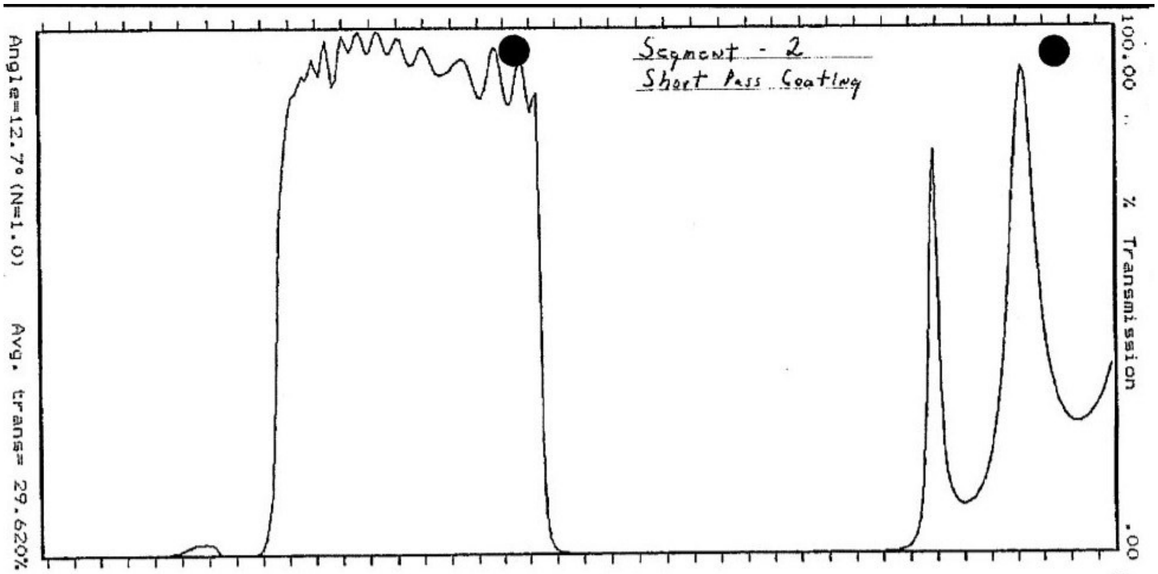

Wavelength	% Refl-N	% Trans-N
6.1000	71.4946	28.5054
5.9500	74.6481	25.3519
5.8000	56.9136	43.0864
5.6500	12.2054	87.7946
5.5000	81.1977	18.8023
5.3500	90.8137	9.1863
5.2000	43.6678	56.3322
5.0500	98.7256	1.2744
4.9000	99.9065	.0935
4.7500	99.9837	.0163
4.6000	99.9957	.0043
4.4500	99.9985	.0015
4.3000	99.9993	.0006
4.1500	99.9996	.0004
4.0000	99.9997	.0002
3.8500	99.9998	.0002
3.7000	99.9997	.0003
3.5500	99.9995	.0005
3.4000	99.9983	.0017
3.2500	99.9864	.0136
3.1000	99.3468	.6532
2.9500	15.7168	84.2832
2.8000	11.3684	88.6316
2.6500	12.8267	87.1733
2.5000	7.4371	92.5629
2.3500	3.3896	96.6104
2.2000	1.6720	98.3280
2.0500	4.2810	95.7167
1.9000	1.1459	98.6876
1.7500	3.2769	92.4822
1.6000	1.0258	85.0315
1.4500	51.8756	1.0790
1.3000	87.0415	.0001
1.1500	38.4983	1.8623
1.0000	37.8872	.5519
.8500	55.2718	.0000
.7000	9.2744	.0000
.5500	46.4262	.0000
.4000	12.3091	.0000
.2500	.0000	.0000

Weight=AVERAGE

Figure 1. VIMS order-sorting/blocking filter transmission for the 1.6-3.0 micron segment. The ringing in the transmission propagates into the radiometric calibration in a complex way because shift in wavelength sample different places in the response function. (From Al-Jumaily, 1991).

VIMS Wavelengths Versus Time

The VIMS calibration pipeline and PDS-delivered data used a wavelength set and FWHM set measured during thermal vacuum testing at JPL before launch (Brown *et al*., 2004), but shifted by 1.3 channels as observed in Galilean Satellite data obtained during the Jupiter flyby (McCord *et al*., 2001). The calibration also incorporated a small, additional set of corrections to a few channels near the wavelength of the 4.25 micron CO_2 absorption (Cruikshank *et al*., 2010). Here we employ terminology to describe the various corrections to the VIMS Radiometric Calibrations by using a numbering scheme RCnn (Radiometric Calibration nn). RC17 was the primary calibration used until June, 2016 (Clark *et al*., 2012), and has been used in all data processed through the VIMS calibration pipeline, and all files delivered to the PDS in the form of calibration files prior to the calibration described herein.

The wavelength calibration shift of the instrument since Cassini's Saturn Orbit Insertion (SOI) is the primary driver of the need to employ a time-dependent radiometric calibration, and has been intensively studied since about 2013. The reader is directed to a separate white paper in the PDS describing the details of the VIMS time-dependent wavelength calibration, which we briefly describe here. Two methods for checking the VIMS wavelengths have been employed: (1) monitoring, as a function of time, the reflectivity in 3 windows of the Titan spectrum (1.6, 2.0, 2.8 microns; see the PDS white paper for details) by fitting Gaussian profiles to the window peaks; and (2) using the VIMS internal, wavelength-calibration, laser diode (central wavelength ~0.979 microns), and employing a fit to the Gaussian intensity profile of the calibration diode convolved with the response of 8 VIMS channels centered near peak intensity of the calibration diode. The result is the derivation of a time-dependent shift of the current wavelengths relative to the set extant at the time of Cassini's SOI. Figures 2, 3 show the results from both methods.

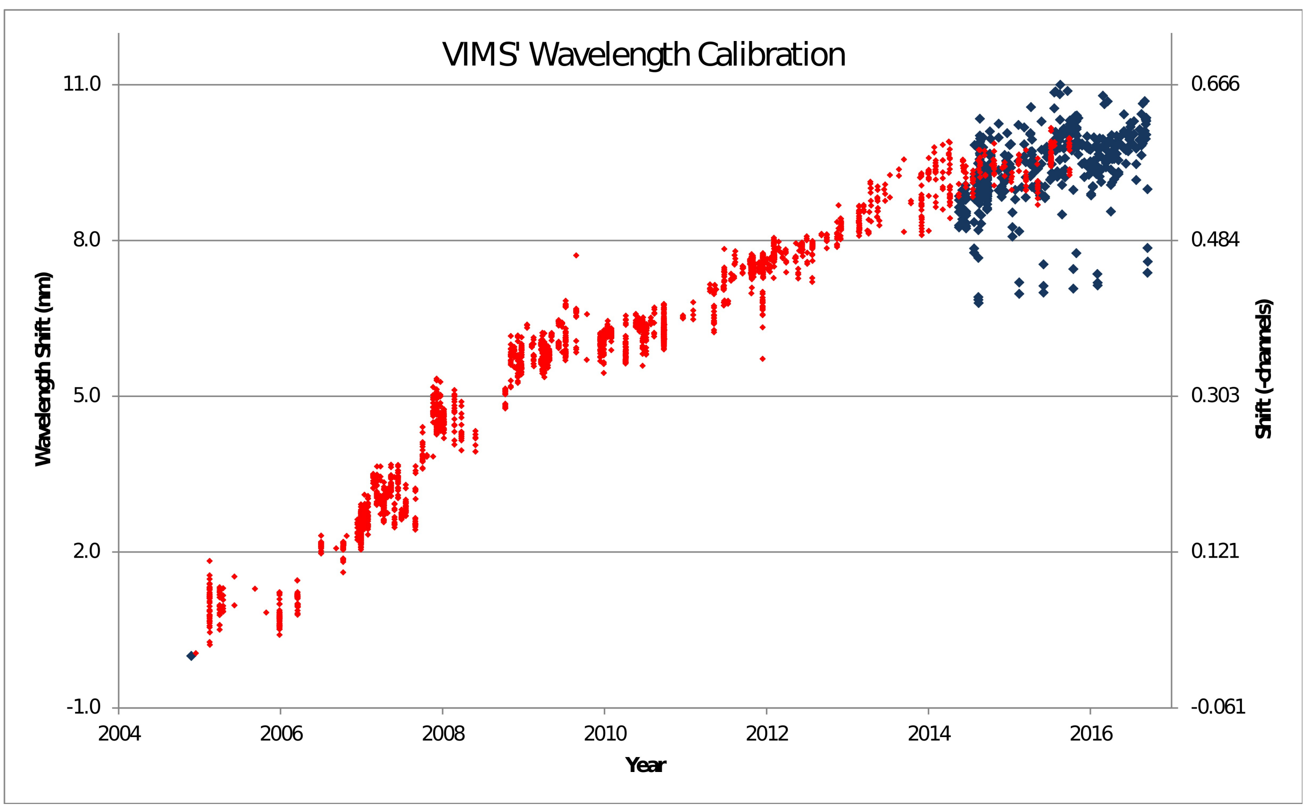

Figure 2. VIMS wavelength shift versus time for two methods: Titan atmospheric windows (red points), and VIMS calibration diode (dark blue points).

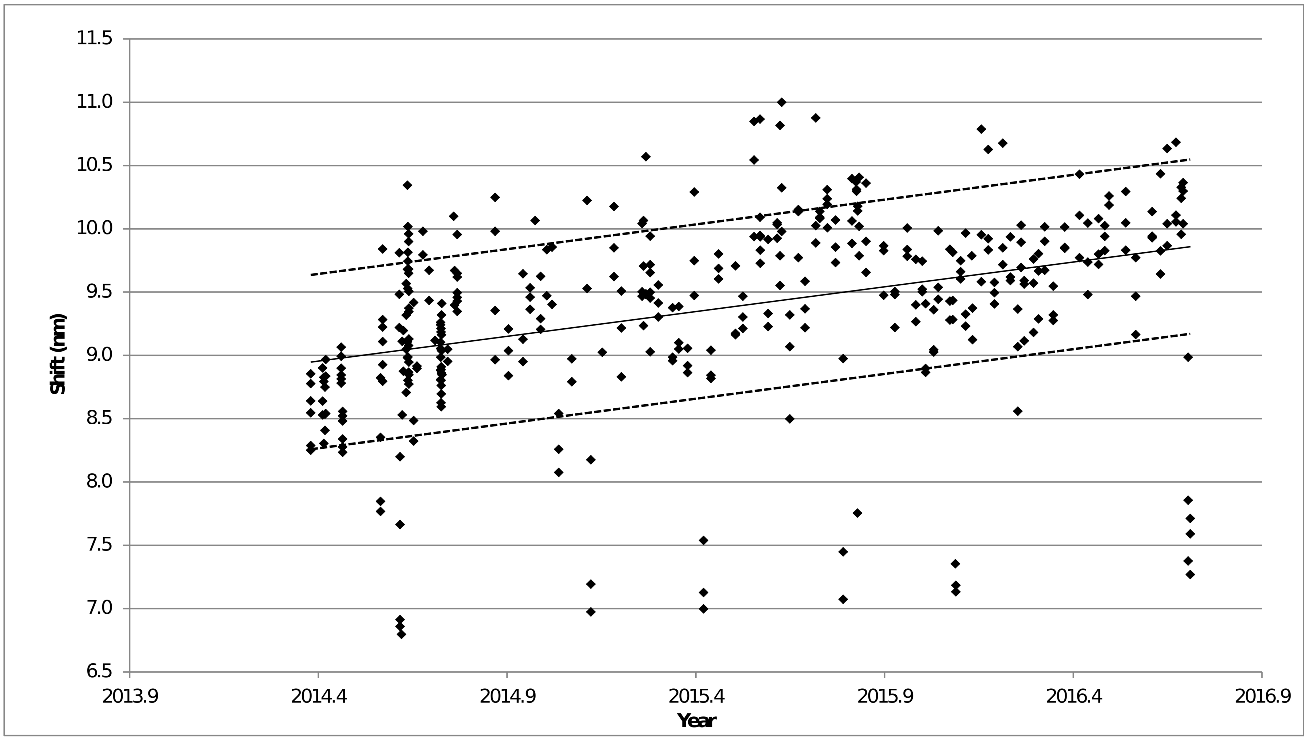

Figure 3. VIMS wavelength shift as measured by the calibration diode. The central, solid line is a linear regression, and the two dotted lines are ± 1 sigma as measured relative to the linear fit. It is not certain if the outlier points indicate real short term variations, but there are some indications that the fluctuations may be caused by temperature cycling of the VIMS spectrometer optics (see PDS white paper).

Because the shifts are small, we specify the shift on a yearly basis as described in Table 1. The shifts are relative to the new "standard 2004.0" wavelengths given in Table 2.

Calibration Equations

The basic equation we employ for calibrated, specific intensity, I, at one wavelength is:

$$I = \frac{\left(R_{DN} - Dark\right)}{flat} CB, \tag{1}$$

where R_{DN} is the instrument raw data number in a given exposure, Dark is the instrument measured dark current and thermal background (a dark/thermal background measurement is made after every VIMS scan line using the same exposure time), and flat is the VIMS flat-field response at the given wavelength and position within the field of view normalized to the response of the boresight pixel (i.e., the relative response of the boresight pixel in the flat-field cube is 1 at every wavelength). The units of equation 1 are: energy/time/area/bandpass/steradian.

C is defined as the calibration-multiplier vector which includes system transmission, grating efficiency, detector response, and divided by the exposure time (see equations 4a and 4b, below).

(2) $$B = \frac{hc}{\lambda\, A\, \Omega\, \Delta\lambda}\ ,$$

where
λ = wavelength,
$\Delta\lambda$ = full width, half maximum, FWHM,
Ω = solid angle = 2.5×10^{-7} steradian,
A = aperture area IR: A = 96.1 cm^2, = 0.00961 m^2 , VIS: A = 15.88 cm^2, A = 0.001588 m^2,
c = speed of light = 2.998×10^{10} cm/s = 2.998×10^{8} m/s, and
h = Planck constant = 6.626×10^{-27} erg-s = 6.626×10^{-34} J-s (= W s^2).

The calibration to apparent reflectance, I/F, referred to that of a Lambert disk (a perfect diffuse reflector) is (note that the factor of π comes from the result that I/F for a Lambert disk is π^{-1}):

(3) $$\frac{I}{F} = \pi \frac{\left(R_{DN} - Dark\right)}{flat} \times \frac{CB}{S}\ ,$$

where t is the exposure time – 0.004 second for the IR, or just the exposure time in seconds for the VIS channel, and S is the solar spectrum from Thompson *et al*. (2015), corrected to the flux extant at the heliocentric distance of the object in question. The 4 millisecond IR exposure time correction is due to settling time after each mirror movement of the scanning secondary and was derived by McCord *et al*., (2004).

In the VIMS instrument, A and Ω are more complex (see Brown *et al.*, 2005). In standard resolution mode, the VIS channel bins 3x3 pixels to make a 0.5 x 0.5 mradian IFOV, and the IR IFOV is actually 0.5 x 0.25 mradian which gets moved 0.25 mradian half way through the integration to make a 0.5 x 0.5 mradian square pixel. In high resolution mode, the VIS channel is 0.17 x 0.17 and the IR is 0.5 x 0.25 mradian. The full telescope aperture, a 22.9 cm diameter Ritchey Cretien telescope, 800-mm focal length, has obscuration in both the Ritchey-Cretien secondary, and in the inverse Dahl-Kirkham collimator and Cassegrain spectrometer optics. We use different constants to scale the relative multiplier (equation 4, below) to compensate for these factors to derive the value of C for each VIS and IR channel and each wavelength.

Derived Spectral Properties

The wavelength calibration and FWHM for VIMS were measured on the ground in a thermal vacuum chamber before launch (Brown *et al.*, 2005). At the Jupiter fly-by it was determined that the IR wavelengths had shifted 1.3 channels from the ground calibration (McCord *et al*., 2001). That 1.3-channel shift from the ground calibration defined the VIMS standard wavelengths for post launch to RC17. No apparent shift occurred after the Jupiter fly-by and before Saturn orbit insertion.

Using the measured wavelength shifts from Table 1 we modeled the effect of the shift on solar port data from 2005 to 2012 (Figure 4). The model does not include order-sorting/blocking-filter response. Unfortunately, as the data in Figure 1 show, the analog plot of filter transmission made over 20 years ago is not precise enough for tracking the effects of the wavelength shifts.

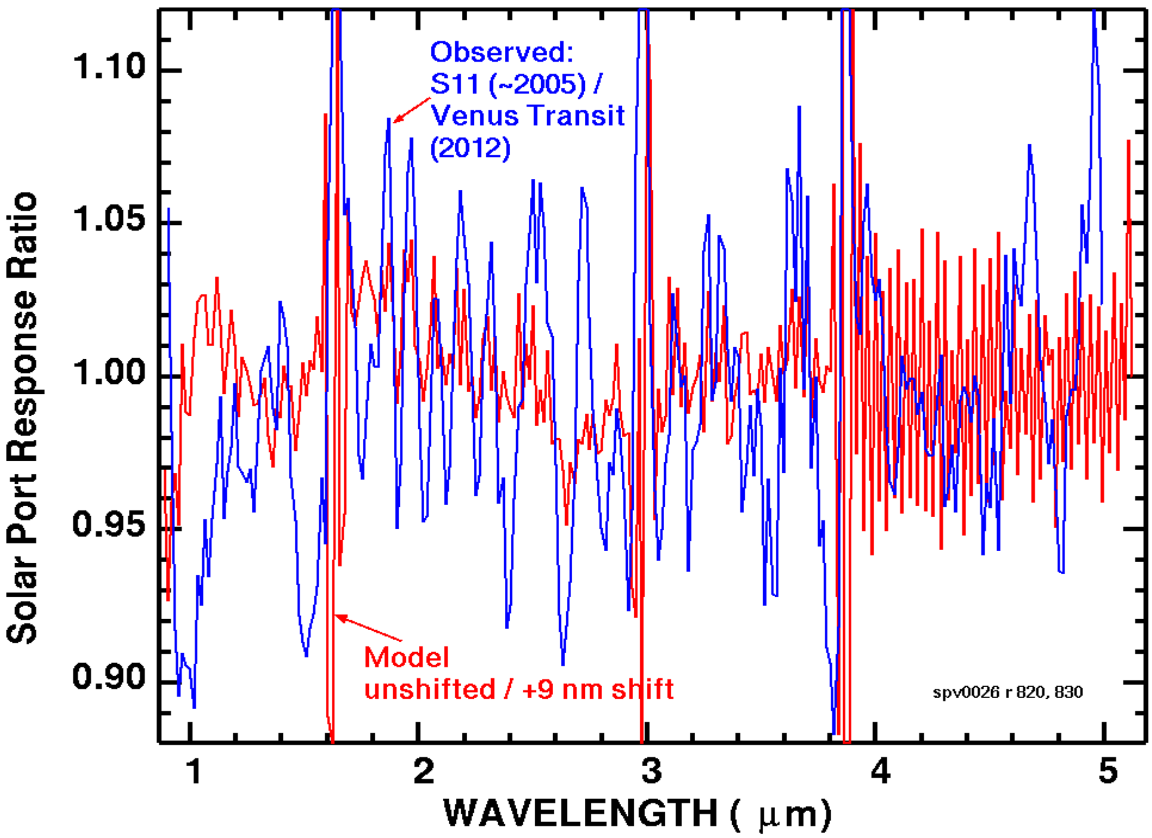

Figure 4: Solar port data from 2005 divided by data from 2012 (blue line) shows larger than predicted changes than just due to solar spectral structure.

Investigation of the causes of the discrepancy shown in Figure 4 revealed that, besides ringing in the order sorting filter transmission, fine structure in the original measured wavelengths of each vims channel and the derived FWHM display periodic structure which we traced to a periodic error in the grating position of the test monochromater used in the ground-based, thermal-vacuum testing of VIMS. Figures 5 and 6 show the trends.

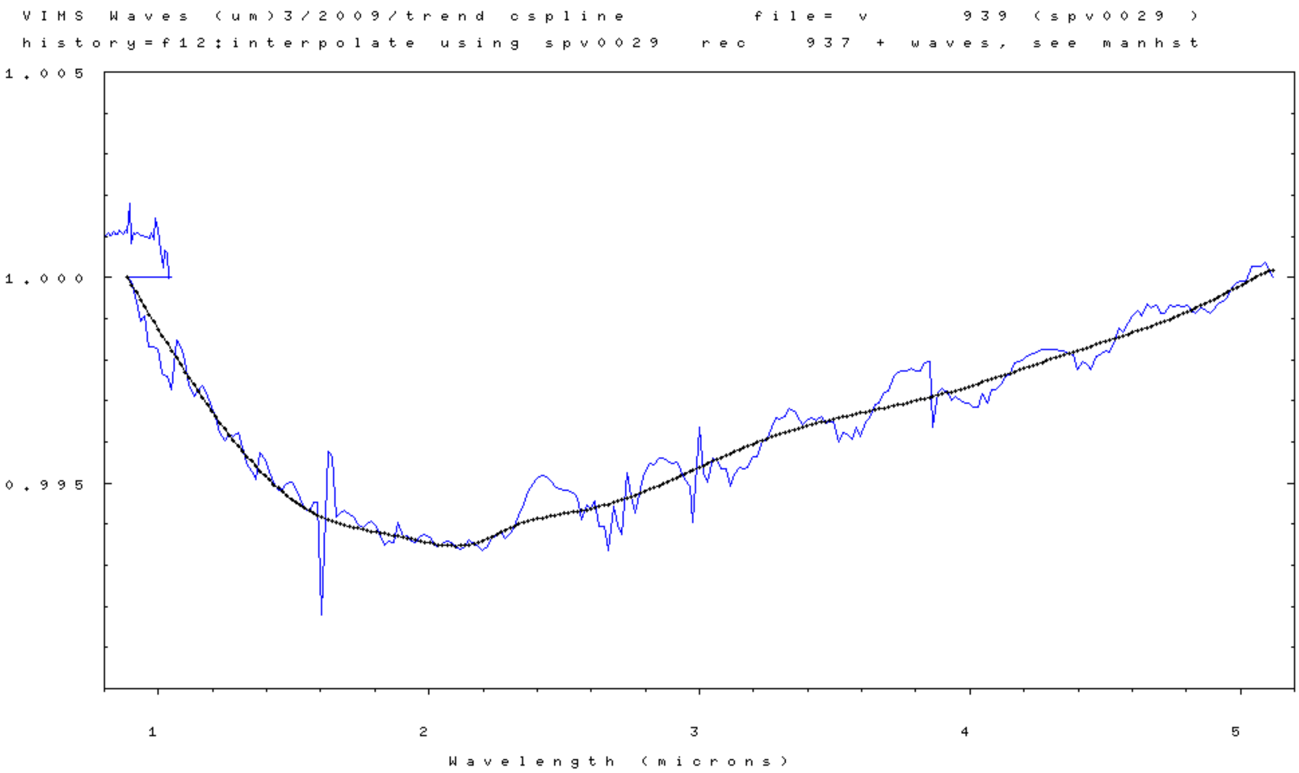

Figure 5. VIMS IR wavelengths divided by a linear fit to the end channels of the IR spectrometer (blue line). A cubic-spline fit (black line) is our new derivation: the new RC19 2004.0 “standard” wavelength set (values in Table 2). The blue line is a plot of the wavelengths derived in thermal vacuum testing before launch and shifted 1.3 channels (derived that the Jupiter fly-by) with a correction for the wavelengths around the 4.25 micron CO_2 atmospheric absorption (Cruikshank *et al*. 2010).

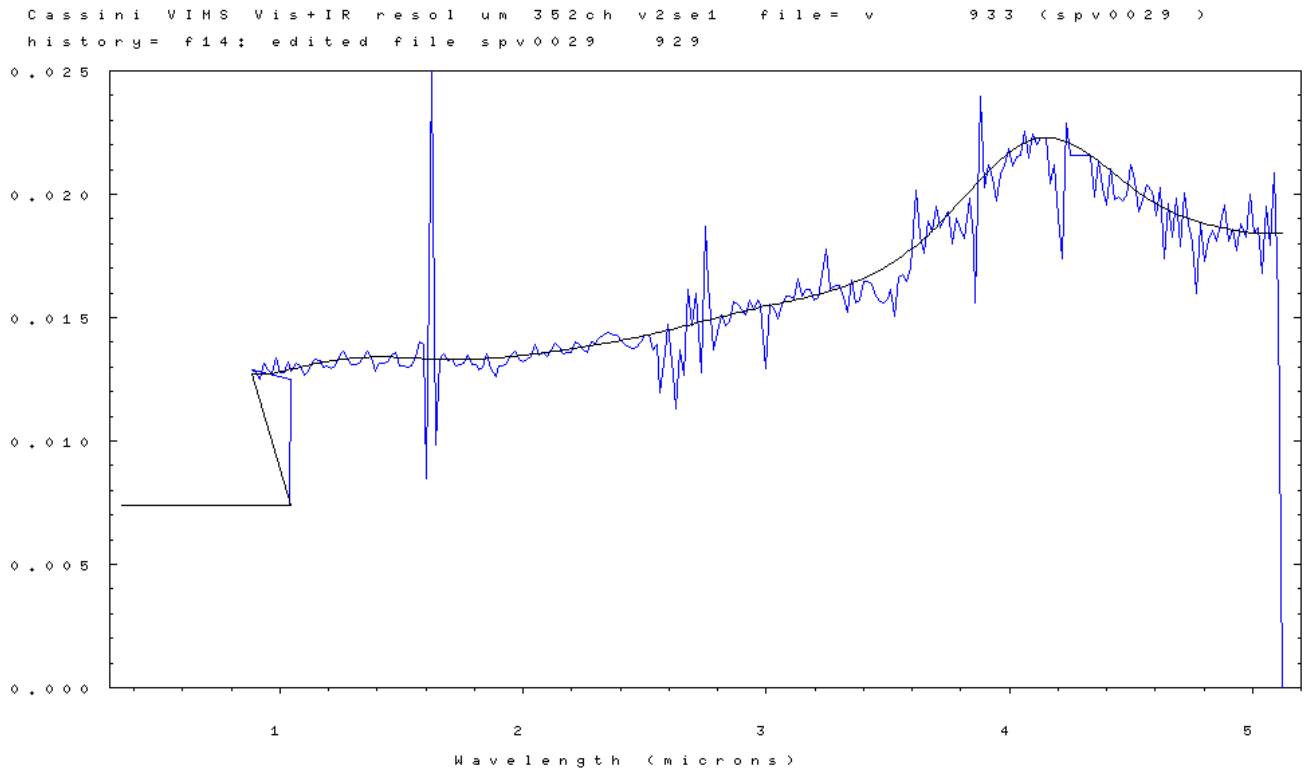

Figure 6. VIMS IR-channel bandpasses (FWHM) in microns (blue line) derived during thermal vacuum testing before launch. A cubic-spline fit (black line) defines the new RC19 FWHM set (values in Table 2).

Calibration Multiplier

The calibration multiplier vector, C, from equation 1 is the major factor that remains to be determined. Ideally it could be derived from measurements of a known, standard reflector illuminated with a source of known intensity, such as a calibration target on the spacecraft illuminated by the Sun, but such a device was descoped from VIMS in early Cassini budget cuts, thus we are left with only more approximate methods. Standard stars (that is, stars whose spectral specific intensities are known with the required precision) could be used, but because they are sub-pixel to VIMS, and because the VIMS pixel response function is variable within a pixel, unresolved objects like stars cannot be used with sufficient accuracy. Therefore, the only practical avenue that remains involves the use of known spectra of Saturn’s icy satellites and rings, Saturn itself, and Titan. Using a cross correlation of the spectra of the various objects, we were able to ascertain in general which “bumps and wiggles” in the response function were instrument related, and which were real features in the spectra of the various objects.

Furthermore, because the reflection spectra of solar-systems objects can be strong functions of their illumination geometry, the spectra of some objects were analyzed as a function of phase angle. For example, high-phase observations of Saturn's D and F-rings are expected to be dominated by diffraction, with muted spectral signatures of water ice, except near the water-ice vibrational fundamentals, where the real index of refraction becomes close to 1.0. The derived, relative-multiplier vector for 2004.0 is shown in Figure 7.

VIMS has order-sorting filter gaps near 1.65, 3, and 3.9 microns (the upward spike in Figure 7), and they do not shift with time because they are fixed with respect to the detector array, whereas the spectrum of an object projected onto the detector array changes with time, and thus all other structure in spectral measurements does change in the IR channel of VIMS. The sampled wavelengths of the visible channel do not shift, thus its ground calibration is sufficient for calibration of the visible-channel data. The VIMS-IR multiplier vector (excluding the filter gap transmission) from Figure 7 was cubic-spline interpolated to the wavelength set derived for each year and given in Table 1. We then applied the effects of the filter-gap transmission.

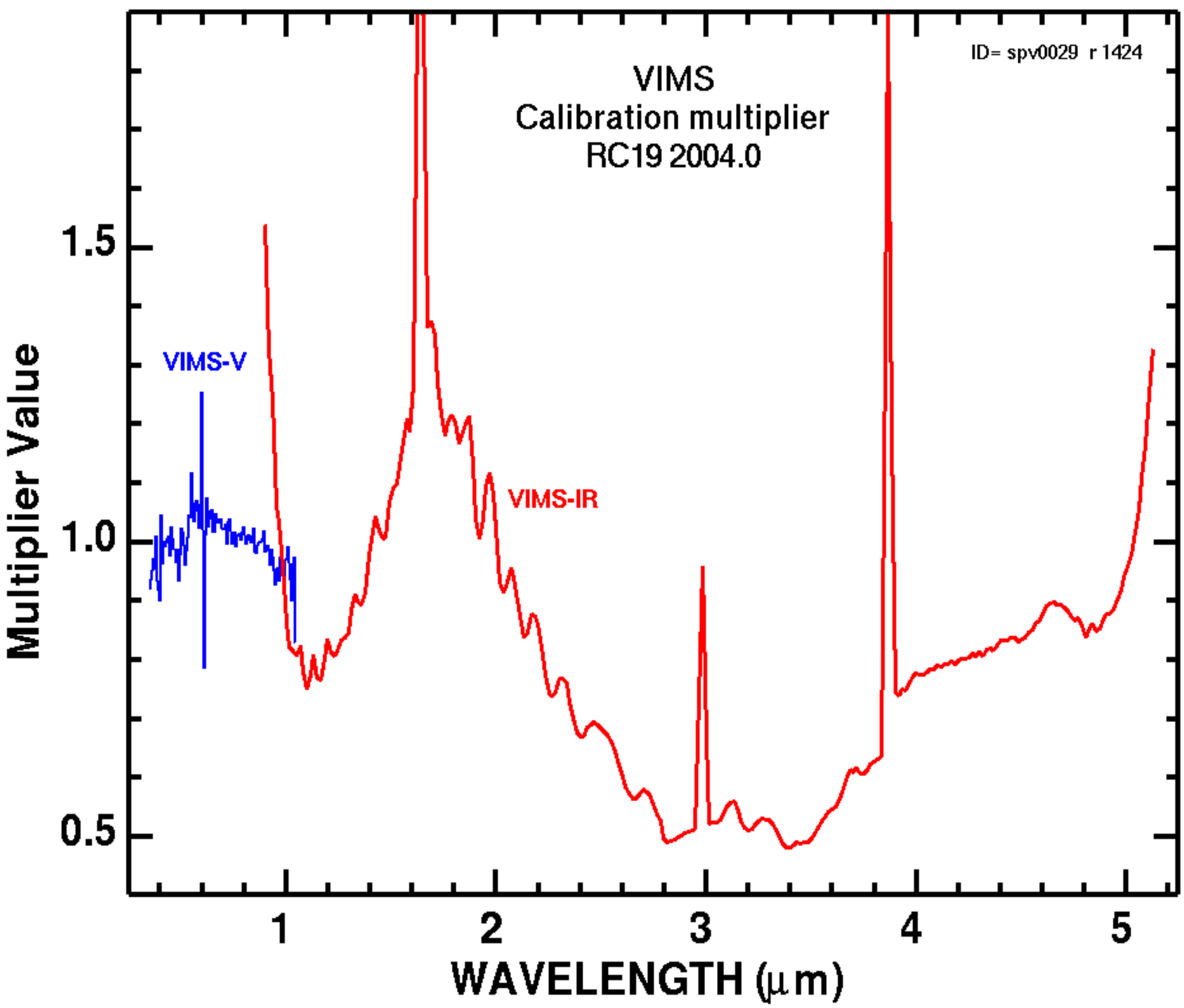

Figure 7. The relative calibration multiplier set for year 2004.0, used in Equation 4. The vector is resampled with time as described in the text.

The results of the new calibration are illustrated in Figure 8. The RC17 calibration, which does not take into account the effects of shifting wavelengths shows increasing ringing (compare The D-ring 2006 RC 17 with F-ring 2015 RC17 spectra). The new RC19 calibration, which tracks the effects of the shifting wavelength sets, eliminates the ringing problems.

Remaining issues and uncertainties include:

1) The small rise near 2.75 microns may or may not be real.

2) The feature near 3 microns is on the edge of the order sorting filter gap and may or may not be real. If real the feature is most likely due to an N-H stretch (e.g. ammonia or ammonium compound).

3) The filter gap transmission around 1.65 and 3.9 microns may need adjustment

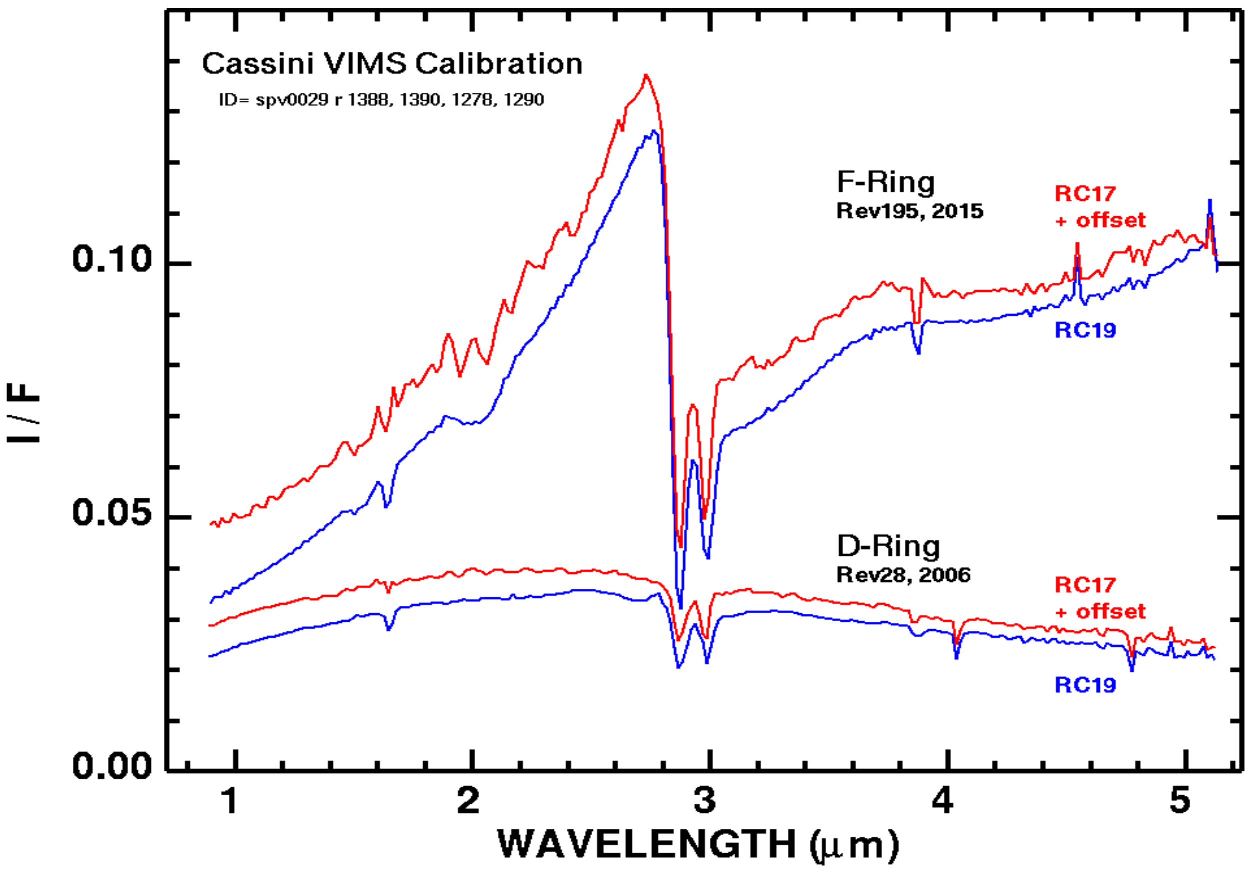

Figure 8. Example VIMS spectra using RC17 which was constant with time, and the new RC19 method described here.

Application/implementation of the time-dependent transfer functions to calibration of data

Calibration of VIMS uses equation 3, above. The value of B from equation 2 is computed by selecting the wavelengths and FWHM for the time of the observation, and MKS units as follows.

$\Omega = 2.5\text{x}10^{-7}$ steradian.
$c = 2.998\text{x}10^{8}$ m/s.
$A = 0.00961$ m^2 (VIS), 0.001588 m^2 (IR).
$h = 6.626\text{x}10^{-34}$ J-s (= W s^2).

λ = wavelength in meters (ascii listings are in microns. So divide by 1000.0).
$\Delta\lambda$ = FWHM in microns.

ASCII listing of the value of B for each VIMS channel is given in the Appendix.

In equation 3,

(4a) C_{VIS} = 29554. * calibration multiplier set from the appendix / (t * gain),

(4b) C_{IR} = 8112. * calibration multiplier set from the appendix / (t * gain),

the calibration multiplier set is one of the files with a name of
vims.calibration.multiplier.RC19-20NN.N.txt
where 20NN.N is the year. The constants in 4a and 4b apply to both standard and high resolution modes. Almost all VIMS observations have been carried out with gain = 1.

The Thompson *et al*. (2015) solar spectra convolved to VIMS are also given in the Appendix for each wavelength and calibration multiplier set.

The resulting units from equation 3 are dimensionless (I/F). To get to radiance, multiply by the solar spectrum. The supplied VIMS-convolved solar spectra are in units of Watts / m^2 / micron.

Plans for 2017-EOM

Wavelength calibration measurements using the instrument's calibration diode will continue to be made every few days until the end of the Cassini mission. When all of the data regarding the shifts are collected, we will then derive a final set of wavelengths which will cover each year during the Cassini Orbital Tour. From those wavelengths will be derived the time-dependent calibration vectors to be applied to all of the VIMS raw data gathered during the Cassini Orbital tour. Those results will be deposited in the PDS 3-6 months after the end of the Cassini Mission. No further analysis will be carried out by the VIMS Team after the end of the Cassini Mission.

Appendices

A tar file, vims-calibration+wavelengths-vs-time-files.tar, contains ascii listings of the wavelengths, calibration multiplier, the computed B values (equation 2), and the VIMS-convolved solar spectrum as a function of time. The time increment is 1 year centered mid year. The VIMS wavelength shift is small enough that this granularity is sufficient for most applications, as the shift between these calibrations is less than 0.0 channel.

Conclusions

The VIMS wavelengths are shifting small amounts per year (less than 0.1 channel), necessitating the need for a time-dependent calibration. We have derived a new methodology that tracks this change and produces significantly better spectra with lower noise and lower artifacts. This new calibration should enable greater confidence in observed spectral features, leading to detection of lower abundance components and therefore new and better science.

Table 1

Time	Shift (nm)	Shift Channels	Add to standard wavelength set: (microns)
2004.0	0.0	0.000	0.0000 (= standard wavelength set)
2005.5	0.4	0.022	0.0004
2006.5	1.9	0.114	0.0019
2007.5	3.4	0.206	0.0034
2008.5	4.9	0.299	0.0049
2009.5	6.0	0.369	0.0060
2010.5	6.0	0.369	0.0060
2011.5	7.0	0.431	0.0070
2012.5	7.7	0.474	0.0077
2013.5	8.4	0.517	0.0084
2014.5	9.0	0.557	0.0090
2015.5	9.7	0.606	0.0097
2016.5	10.4	0.650	0.0104
2017.5	11.1	0.694	0.0111 (projected)

Table 2

VIMS Standard Wavelengths (2004.0)

	Standard wavelength (microns)	FWHM (microns)
1	0.350540	0.007368
2	0.358950	0.007368
3	0.366290	0.007368
4	0.373220	0.007368
5	0.379490	0.007368
6	0.387900	0.007368
7	0.395180	0.007368
8	0.402520	0.007368
9	0.409550	0.007368
10	0.417310	0.007368
11	0.424360	0.007368
12	0.431840	0.007368
13	0.439190	0.007368
14	0.446520	0.007368
15	0.453720	0.007368
16	0.461630	0.007368
17	0.468410	0.007368
18	0.476220	0.007368
19	0.486290	0.007368
20	0.489670	0.007368
21	0.497770	0.007368
22	0.506280	0.007368
23	0.512220	0.007368

24	0.519630	0.007368
25	0.527660	0.007368
26	0.534160	0.007368
27	0.541560	0.007368
28	0.549540	0.007368
29	0.556140	0.007368
30	0.563530	0.007368
31	0.571310	0.007368
32	0.578100	0.007368
33	0.585480	0.007368
34	0.593120	0.007368
35	0.599380	0.007368
36	0.607570	0.007368
37	0.615050	0.007368
38	0.622070	0.007368
39	0.629400	0.007368
40	0.637040	0.007368
41	0.644080	0.007368
42	0.651420	0.007368
43	0.659100	0.007368
44	0.666090	0.007368
45	0.673420	0.007368
46	0.681020	0.007368
47	0.688030	0.007368
48	0.695350	0.007368
49	0.702880	0.007368
50	0.710000	0.007368
51	0.717330	0.007368
52	0.724840	0.007368
53	0.731980	0.007368
54	0.739300	0.007368
55	0.746760	0.007368
56	0.753960	0.007368
57	0.761280	0.007368
58	0.768740	0.007368
59	0.775950	0.007368
60	0.783280	0.007368
61	0.790720	0.007368
62	0.797930	0.007368
63	0.805220	0.007368
64	0.812620	0.007368
65	0.819890	0.007368
66	0.827210	0.007368
67	0.834630	0.007368
68	0.841900	0.007368
69	0.849220	0.007368
70	0.856630	0.007368
71	0.863910	0.007368
72	0.871220	0.007368

73	0.878630	0.007368	
74	0.885890	0.007368	
75	0.893860	0.007368	
76	0.900320	0.007368	
77	0.907870	0.007368	
78	0.915180	0.007368	
79	0.922540	0.007368	
80	0.929830	0.007368	
81	0.937130	0.007368	
82	0.944450	0.007368	
83	0.951770	0.007368	
84	0.959070	0.007368	
85	0.966380	0.007368	
86	0.973820	0.007368	
87	0.981000	0.007368	
88	0.988830	0.007368	
89	0.995880	0.007368	
90	1.002950	0.007368	
91	1.010050	0.007368	
92	1.016950	0.007368	
93	1.024710	0.007368	
94	1.031950	0.007368	
95	1.038650	0.007368	
96	1.045980	0.012480	End of VIS channel
97	0.884210	0.012878	
98	0.900753	0.012767	
99	0.916924	0.012507	
100	0.933078	0.013169	
101	0.949803	0.012869	
102	0.965683	0.012728	
103	0.982262	0.013370	
104	0.998820	0.012790	
105	1.014790	0.012748	
106	1.031320	0.013186	
107	1.047550	0.012847	
108	1.065410	0.013136	
109	1.081830	0.013063	
110	1.098060	0.012686	
111	1.113960	0.012828	
112	1.130240	0.013111	
113	1.146950	0.013322	
114	1.163700	0.013266	
115	1.179960	0.012968	
116	1.196220	0.013018	
117	1.212460	0.012921	
118	1.228590	0.013031	
119	1.244920	0.013401	
120	1.261660	0.013631	
121	1.278130	0.013372	

122	1.294820	0.013121	
123	1.310910	0.013101	
124	1.326950	0.013146	
125	1.343240	0.013389	
126	1.359520	0.013663	
127	1.376950	0.013366	
128	1.393260	0.012821	
129	1.409400	0.013147	
130	1.425570	0.013137	
131	1.441840	0.013216	
132	1.458410	0.013480	
133	1.475140	0.013610	
134	1.491690	0.013066	
135	1.507940	0.013063	
136	1.524210	0.012992	
137	1.540350	0.013059	
138	1.556740	0.013388	
139	1.573610	0.014011	
140	1.590180	0.013901	
141	1.602280	0.008457	order-sorting filter change
142	1.625230	0.032000	order-sorting filter change
143	1.641600	0.009862	order-sorting filter change
144	1.655670	0.013304	
145	1.672380	0.013532	
146	1.689010	0.013253	
147	1.705360	0.013300	
148	1.721750	0.013068	
149	1.738020	0.013084	
150	1.754360	0.013155	
151	1.771050	0.013455	
152	1.787710	0.013080	
153	1.804010	0.013090	
154	1.820040	0.012902	
155	1.836160	0.012985	
156	1.852880	0.013531	
157	1.869330	0.012939	
158	1.886790	0.012600	
159	1.902610	0.013058	
160	1.919160	0.013059	
161	1.935450	0.013127	
162	1.951910	0.013498	
163	1.968710	0.013615	
164	1.985310	0.013293	
165	2.001670	0.013209	
166	2.017810	0.013294	
167	2.034240	0.013415	
168	2.050910	0.013889	
169	2.067570	0.013472	
170	2.084000	0.013579	

171	2.100340	0.013428
172	2.116670	0.013719
173	2.133370	0.013943
174	2.150180	0.013787
175	2.166520	0.013547
176	2.182880	0.013600
177	2.199200	0.013571
178	2.215910	0.014009
179	2.232820	0.013918
180	2.249520	0.013700
181	2.266220	0.013600
182	2.282380	0.014012
183	2.299210	0.013974
184	2.316120	0.014211
185	2.333250	0.014287
186	2.350430	0.014407
187	2.367650	0.014286
188	2.384720	0.014294
189	2.401560	0.014079
190	2.418200	0.013921
191	2.434710	0.013829
192	2.450970	0.013748
193	2.467230	0.013784
194	2.483600	0.014044
195	2.500020	0.014293
196	2.516590	0.014306
197	2.532920	0.013704
198	2.549160	0.013918
199	2.564370	0.011963
200	2.581760	0.013610
201	2.598070	0.014726
202	2.615080	0.012722
203	2.630000	0.011283
204	2.646500	0.013711
205	2.661460	0.012674
206	2.680850	0.016119
207	2.696200	0.014697
208	2.712050	0.015964
209	2.732700	0.012786
210	2.747700	0.018701
211	2.763050	0.016296
212	2.781180	0.013689
213	2.798890	0.014400
214	2.816060	0.015083
215	2.832470	0.014680
216	2.849540	0.014842
217	2.866090	0.015667
218	2.882420	0.015534
219	2.898780	0.015325

220	2.915400	0.015088	
221	2.931430	0.015720	
222	2.947260	0.015350	
223	2.963270	0.015716	order-sorting filter change
224	2.977200	0.015512	order-sorting filter change (~30% transmission)
225	3.000720	0.012919	order-sorting filter change
226	3.013820	0.015570	
227	3.029700	0.015398	
228	3.048060	0.014922	
229	3.064460	0.015466	
230	3.080360	0.015882	
231	3.096890	0.015851	
232	3.112130	0.015753	
233	3.129620	0.016580	
234	3.146670	0.015851	
235	3.163040	0.016127	
236	3.179740	0.016115	
237	3.197080	0.015685	
238	3.213640	0.015830	
239	3.231500	0.016740	
240	3.248060	0.017771	
241	3.265610	0.016161	
242	3.282980	0.016285	
243	3.299460	0.016286	
244	3.316190	0.015816	
245	3.333380	0.015203	
246	3.349810	0.016500	
247	3.365640	0.015590	
248	3.381830	0.015717	
249	3.398720	0.016471	
250	3.415460	0.016457	
251	3.431780	0.016343	
252	3.448740	0.015852	
253	3.464750	0.015634	
254	3.481370	0.015608	
255	3.497950	0.015779	
256	3.512840	0.016141	
257	3.530150	0.015057	
258	3.546640	0.016643	
259	3.562740	0.016735	
260	3.580340	0.016474	
261	3.596100	0.017033	
262	3.613870	0.020159	
263	3.630850	0.018293	
264	3.648530	0.017622	
265	3.665220	0.018895	
266	3.682830	0.018505	
267	3.699530	0.019496	
268	3.717430	0.018635	

269	3.734390	0.019045	
270	3.751030	0.019296	
271	3.767630	0.017966	
272	3.784440	0.019006	
273	3.800830	0.018599	
274	3.817420	0.018210	
275	3.834720	0.019856	
276	3.851410	0.018125	
277	3.861840	0.015574	order-sorting filter change
278	3.881670	0.023959	order-sorting filter change
279	3.898590	0.020270	
280	3.914780	0.021217	
281	3.930690	0.020631	
282	3.947620	0.019721	
283	3.963750	0.020799	
284	3.980150	0.021142	
285	3.996720	0.021846	
286	4.012800	0.021142	
287	4.029440	0.021531	
288	4.047300	0.021598	
289	4.062950	0.022566	
290	4.080861	0.021479	
291	4.097430	0.022433	
292	4.114500	0.022013	
293	4.131830	0.022290	
294	4.148830	0.022294	
295	4.166440	0.020424	
296	4.183199	0.021180	
297	4.200100	0.019057	
298	4.217000	0.017383	
299	4.233700	0.022866	
300	4.250500	0.021600	
301	4.267300	0.021600	
302	4.284000	0.021600	
303	4.300600	0.021600	
304	4.317101	0.021600	
305	4.333600	0.021600	
306	4.350200	0.019916	
307	4.366500	0.021335	
308	4.382900	0.020260	
309	4.397930	0.019563	
310	4.415370	0.021034	
311	4.431720	0.019802	
312	4.447720	0.019867	
313	4.465730	0.019735	
314	4.482400	0.019931	
315	4.499511	0.021189	
316	4.515910	0.020529	
317	4.533790	0.019303	

318	4.551870	0.019921	
319	4.567970	0.020376	
320	4.585560	0.020113	
321	4.602900	0.019105	
322	4.620100	0.020267	
323	4.636150	0.017409	
324	4.654160	0.019612	
325	4.670340	0.018281	
326	4.687210	0.019814	
327	4.702900	0.017902	
328	4.719561	0.020080	
329	4.737060	0.018831	
330	4.753510	0.018017	
331	4.770310	0.015955	hot pixel
332	4.786730	0.018821	
333	4.803490	0.017274	
334	4.819521	0.018179	
335	4.835771	0.018545	
336	4.852920	0.018106	
337	4.869401	0.018799	
338	4.885530	0.019556	
339	4.902650	0.018114	
340	4.919831	0.018570	
341	4.936851	0.017740	slightly noisier (1.5x at low signal)
342	4.953890	0.018779	
343	4.971780	0.018266	
344	4.988960	0.020001	
345	5.005760	0.018402	
346	5.022400	0.018621	
347	5.040781	0.016783	
348	5.057340	0.019510	
349	5.074020	0.017953	
350	5.091060	0.020883	slightly noisier (2x at low signal)
351	5.106800	0.015704	
352	5.122500	0.016	

References

Al-Jumaily, G.A., E. Miller, and N. Raof, 1991, C/C VIMS Filter requirements, JPL VIMS Design File Memorandum, 6-25-1991.

Brown, R.H., Baines, K.H., Bellucci, J.P., Bibring, B.J., Buratti, E., Bussoletti, F., Capaccioni, P., Cerroni, P., Clark, R.N., Coradini, D.P., Cruikshank, P., Drossart, Y., Formisano, R., Jaumann, Y., Langevin, D.J., Matson, T.R., 2005, The Cassini visual and infrared mapping spectrometer investigation: *Space Science Reviews*, **115 (1-4)**, 111-168.

Clark, R. N., D. P. Cruikshank, R. Jaumann, R. H. Brown, K. Stephan, C. M. Dalle Ore, K. E. Livo, N. Pearson, J. M. Curchin, T. M. Hoefen, B. J. Buratti, G. Filacchione, K. H. Baines, and P. D. Nicholson, 2012, The Composition of Iapetus: Mapping Results from Cassini VIMS, *Icarus*, **218**, 831-860.

Cruikshank, D. P., A. W. Meyerb and, R. H. Brownc and, R. N. Clark, R. Jaumann, K. Stephan, C. A. Hibbitts, S. A. Sandford, R. M.E. Mastrapa, G. Filacchione, C. M. Dalle Ore, P. D. Nicholson, B. J. Buratti, T. B. McCord, R. M. Nelson, J. B. Dalton, K. H. B., and D. L. Matson, 2010, Carbon dioxide on the satellites of Saturn: Results from the Cassini VIMS investigation and revisions to the VIMS wavelength scale, *Icarus*, **206**, 561–572, doi:10.1016/j.icarus.2009.07.012 .

McCord, T. B., Brown, R., Baines, K., Bellucci, G., Bibring, J.-P., Buratti, B., Capaccioni, F., Cerroni, P., Clark, R.N., Coradini, A., Cruikshank, D., Drossar, P., Formisano, V., Jaumann, R., Langevin, Y., Matson, D., Mennella, V., Nelson, R., Nicholson, P., Sicardy, B., Sotin, C., Hansen, G., Hibbitts, C., 2004, Cassini VIMS observations of the Galilean satellites, including the VIMS calibration procedure: *Icarus*, Vol. 172, p. 104-126.

Miller, Edward A., Gail Klein, David W. Juergens, Kenneth Mehaffey, Jeffrey M. Oseas, Ramon A. Garcia, Anthony Giandomenico, Robert E. Irigoyen, Roger Hickok, David Rosing, Harold R. Sobel, Carl F. Bruce, Jr., Enrico Flamini, Romeo DeVidi, Francis M. Reininger, Michele Dami, Alain Soufflot, Yves Langevin, Gerard Huntzinger, 1996, The Visual and Infrared Mapping Spectrometer for Cassini , *Proc. SPIE* **2803**, *Cassini/Huygens: A Mission to the Saturnian Systems*, 206-220 (October 7, 1996), doi: 10.1117/12.253421 .

Thompson, D. R., F. C. Seidel, B. C. Gao, M. M. Gierach, R. O. Green, R. M. Kudela, and P. Mouroulis , 2015, Optimizing irradiance estimates for coastal and inland water imaging spectroscopy, *Geophys. Res. Lett.*, **42**, 4116–4123, doi:10.1002/2015GL063287.